



Microstructure, mechanical property and wear behavior of AlCrFe1.5Ni1.5 medium entropy alloy

Ling Qiao¹ and Jingchuan Zhu^{1,*}

¹School of Material Science and Engineering, Harbin Institute of Technology, Harbin 150001, Heilongjiang, China

Received: 8 December 2021

Accepted: 7 June 2022

Published online:
28 June 2022

© The Author(s), under exclusive licence to Springer Science+Business Media, LLC, part of Springer Nature 2022

ABSTRACT

In present study, a cost-effective Co-free AlCrFe1.5Ni1.5 medium entropy alloys (MEAs) have been developed by vacuum melting technology. The microstructure of the AlCrFe1.5Ni1.5 MEAs and mechanical characteristics as well as wear behavior were explored in detail. The XRD patterns indicate that the crystal structure of AlCrFe1.5Ni1.5 MEAs includes dual phases of ordered B2 phase and disordered BCC type [Fe, Cr] phase. The lamellar dendritic regions and a spinodal decomposed microstructure can be observed from the microstructural morphology. The TEM analysis of nano structural evolution further identified the formation of Al-Ni-rich B2 phase and Cr-Fe-rich BCC phase with a high degree of coherence. Attributed to the spinodal decomposition of BCC phases, the as-cast AlCrFe1.5Ni1.5 alloy shows the exceptional plasticity (plastic strain > 40%) and fairly high yield strength of 1231.64 MPa and fracture strength of 2172.79 MPa at room temperature. The true strength was 1360.88 MPa, accompanied with a high true strain of 35.44%. Besides, it also shows great work hardening ability and desirable mechanical properties at elevated temperature. The detailed investigation on the wear behavior shows low average friction coefficient and wear volume loss during the dry sliding process. The wear mechanism involves the abrasive and adhesive wear as well as oxidation. As a result, the dual phase strengthening in AlCrFe1.5Ni1.5 MEAs contributes to the excellent mechanical properties and wear resistance.

Introduction

As a breakthrough of traditional steels and metallic materials, high-entropy alloys (HEAs) or medium-entropy alloys (MEAs) were proposed [1, 2] with the

concentrations of each element in equiatomic or near-equiatomic concentrations between 5 and 35 at%. It has also been determined that there are basically four core effect, including thermodynamics, severe distortion of lattice structures, sluggish diffusion (kinetics) as well as cocktail effects, in HEAs/MEAs

Handling Editor: Megumi Kawasaki.

Address correspondence to E-mail: fgms@hit.edu.cn

<https://doi.org/10.1007/s10853-022-07416-0>

which affects microstructures and properties of HEAs [3–5]. Generally, the mixing entropy of multi-component alloys contributes to the presence of solid solutions. The published literatures reveal that single phase HEAs with FCC-type structure usually presents preferable plasticity but low strength while the HEAs with BCC-type structure exhibit low plasticity [6, 7]. Owing to the specific features, the HEAs including microstructures as well as properties have attracted wide attention. For example, the HEAs usually exhibit exceptional mechanical properties [8–13] and various physical properties [14, 15], excellent wear and corrosion resistance [16–19], high thermal stability and oxidation resistance at elevated temperatures [20–24]. Thus, HEAs and MEAs have been considered as a promising candidate for engineering applications and have great potential for development in the future.

With the introduction of the high-entropy concept, an increasingly number of combinations of alloying elements have attracted extensive scientific interests over the past decade. Up to now, many researches on HEAs and MEAs consisting of microstructures as well as exceptional properties have been reported in literature. Lu et al. [25] proposed the eutectic alloy idea to design HEAs to achieve a great combination of strength and ductility. With a mixture of FCC and BCC phases, the AlCoCrFeNi_{2.1} eutectic HEA was designed and prepared which showed excellent mechanical properties. While, most reported high entropy alloys systems contain a large amount of Co element, which produces high costs and limits their engineering application. To effectively address this problem, the Co-free AlCrFeNi type MEAs and HEAs have drawn particular attention. With respect to the Al-Cr-Fe-Ni alloy system, Dong et al. [26] designed the AlCrFe₂Ni₂ alloy based on the AlCoCrFeNi_{2.1} HEA. With the composite effect of the softer FCC and harder BCC phases, the as-cast AlCrFe₂Ni₂ alloy showed excellent mechanical properties which were superior to most HEAs and was even comparable with the Ti-based ultrafine-grain alloy. K.B Kim et al. [27] proposed that the addition of specific minor elements such as Mo and Ti can lead to the variation in volume fraction and grain size on the nanoscale, which can further contribute to the enhancement of mechanical properties and high-temperature hardness behavior of AlCrFeNi eutectic high entropy alloys.

Perhaps the most significant benefit of HEAs/MEAs is that they suggest an enormous number of possible compositions, exhibiting great potential in scientific and practical application [28]. Despite there are increasing researches reported on the HEAs/MEAs, most of scientific works mainly focus on the microstructures and the resulted mechanical properties. As known, the lattice of HEAs is usually distorted due to the chemical bonds of the alloying elements and the variation in atomic sizes [29], thus the HEAs is prone to show high hardness and strength than the conventional metal materials. According to the Archard equation, the wear resistance of a material is proportional to the hardness (or strength) [30]. With the increasingly complex friction conditions, several studies [31, 32] have reported that the HEAs/MEAs are expected to possess great wear resistance. For example, concerning the tribological properties of HEAs, J.W.Qiao et al. [33] investigated the effects of temperature on the tribological behavior of Al_{0.25}CoCrFeNi high-entropy alloy. The results show that the wear rate increased with increasing temperature due to high temperature softening, and then remained stabilized above 300 °C with the anti-wear effect of the oxidation film on the contact interface. The wear mechanism varies with the service temperature. K.M Doleker et al. [34] investigated the effect of Cu, Si, Co element on the AlCrFeNi-base HEAs. The highest hardness, highest wear resistance and lowest friction coefficient was obtained in AlCrFeNiSi alloy, which contains BCC phases as well as intermetallic phases. With respect to the Al-Cr-Fe-Ni alloy system, based on the author's previous works [11, 35, 36], the HEAs/MEAs are usually composed of dual phases so that the dual-phase strengthening effect is expected to result in the tribological improvement.

Despite the AlCrFeNi-based MEAs always exhibit high temperature stability, it is limited in developing the components used at ambient temperature due to their room temperature brittleness and deficiency in wear resistances. In this paper, to reduce the cost and further improve the mechanical properties, the new Co-free AlCrFe_{1.5}Ni_{1.5} MEAs was designed and characterized. The AlCrFe_{1.5}Ni_{1.5} MEAs samples are synthesized by vacuum melting method and then the phase formation and microstructural evolution has been briefly studied. Experimental efforts have been made to assess the mechanical properties of AlCrFe_{1.5}Ni_{1.5} MEAs at both ambient and high

temperatures. To evaluate the wear resistance, the present work also attempts to ascertain the sliding wear response of AlCrFe1.5Ni1.5 MEAs at ambient temperature. In particular, this work provides an in-depth insight into the strengthening mechanism and wear mechanism of AlCrFe1.5Ni1.5 MEAs, which can provide theoretical guidance for its practical application.

Experimental procedure

In this work, AlCrFe1.5Ni1.5 MEAs were prepared by vacuum arc melting techniques. With a mixture of high purity ($> 99.99\%$) raw metals under high purity argon atmosphere, the ingot was melted at least five times to ensure the chemical homogeneity. X-ray diffraction (XRD) profiles were then obtained using a XPERT diffractometer with a Cu K α radiation source with the 2θ scan from 10 to 110° . The microstructure characterization was investigated by scanning electron microscopy (SEM) techniques. The SEM samples were pre-treated by mechanical polishing, followed by chemical etching with a mixed solution of $\text{HNO}_3 : \text{HCl} : \text{H}_2\text{O} = 1 : 3 : 4$. Transmission electron microscope (TEM) was used for further identification of phase structure and phase composition. The specimens for TEM observation were ground to the thickness of less than $80 \mu\text{m}$ using mechanical grinding followed by electropolishing.

In the compressive tests, the samples with the diameter of 4 mm and the height of 6 mm were extracted from the ingots. The AG-XPlus 250kN/50kN Electronic Universal Testing Machine was employed with an initial strain rate of 0.5 mm/min at room temperature. For high temperature compressive tests, the strain rate is determined as 2 mm/min. Prior to the compressive tests, the samples were carefully mechanical ground and polished to remove the surface defects.

The friction and wear tests were carried out with a reciprocating ball-on-flat sliding tribometer (CETR-UMT-3). Samples were held on the flat with a constant normal load of 25 N for a duration of 1800 s and the total sliding distance for a typical test was therefore about 5 mm. The sliding speed used in this work is 10 mm/s, and the friction coefficient was measured during each test. The morphology of the wear tracks was investigated by a combination of electron probe microanalysis (EPMA, JXA-8230) and

surface profilometry using a three-dimensional surface topography profiler (Zeta20). EPMA imaging allowed for the investigation of wear mechanisms, while profilometry was used to provide a quantitative measurement of wear volume.

Results and discussion

Phase and microstructure

In general, the material properties are considered a function of phase compositions and microstructure, a systematic understanding towards phase formation and microstructural evolution phenomena is of vital importance. Figure 1 shows the XRD patterns of AlCrFe1.5Ni1.5 MEAs. The pattern reveals that only the BCC diffraction peaks are detected in the alloy. Particularly, the existence of a (100) peak indicates an ordered BCC phase (B2 phase). As a common phenomenon in multi-component alloys, the overlapping peaks can be observed in XRD patterns which indicate the similar crystal structures of ordered (Ni, Al) phase and disordered [Fe, Cr] phase. With respect to the previous study [37], this phenomenon can be ascribed to the spinodal decomposition.

Figure 2 displays the SEM images of the as-cast AlCrFe1.5Ni1.5 MEAs. As Fig. 2a indicates, the lamellar dendritic structure can be observed near the grain boundary. Besides the dendrite structure, bright and dark sections of interconnected microstructures can also be observed within the grains. Figure 2b plots a periodic maze-shaped microstructure at high magnifications, which is a

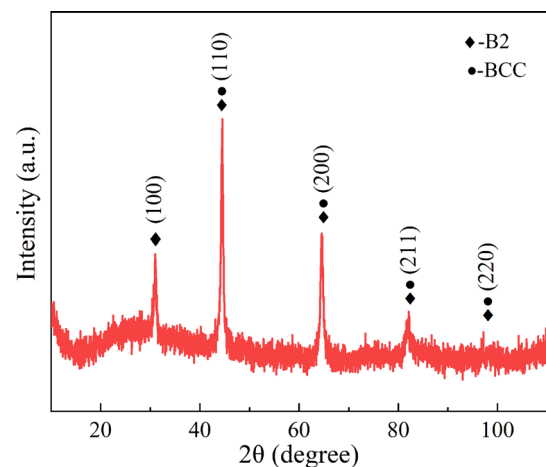
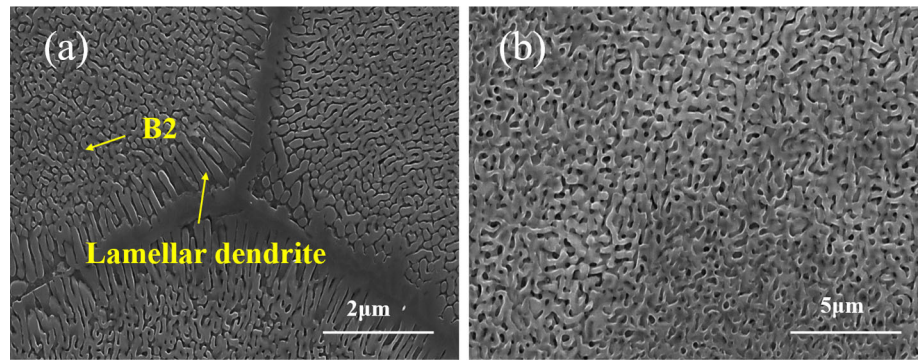


Figure 1 XRD analysis of AlCrFe1.5Ni1.5 MEAs.

Figure 2 Microstructure of AlCrFe1.5Ni1.5 MEAs. **a** The microstructure in high magnification **b** The microstructure within the grains.



typical characteristic of spinodal decomposition [37]. The modulated microstructure confirms the formation of BCC/B2 phase and corresponds to the overlapping disordered BCC [Fe, Cr] phase and B2 bragg reflections in the XRD analysis.

TEM analysis

Figure 3 presents a bright-field TEM micrograph of the as-cast AlCrFe1.5Ni1.5 MEAs. Fig. 3a displays the eutectic microstructure and clearly reveals that the alloy is composed of two alternating phases. Evidently, two kinds of regions can be identified in the microstructure. The selected-area electron diffraction pattern confirms that the eutectic structure is a mixture of Fe-Cr-rich BCC structure and B2 phase. Figure 3b presents the SAED pattern of an Ni-Al-rich region corresponding to the B2 phase along [001] zone axis. Otherwise, Fig. 3c plots the SAED pattern of a Fe-Cr rich region corresponding to the A2 structure phase along [001] zone axis. In terms of the spinodal structures, the B2 phase denotes the inter-precipitate and the precipitated-like particles are BCC phases. Figure 3d displays the element distribution maps detected by TEM-EDS. It indicates that the spherical particles are rich in Fe and Cr and poor in Ni and Al. The inter-precipitate are Fe-Cr-rich phases. As a result, the TEM-EDS results and SAED patterns indicate that the BCC phase is Fe-Cr-rich phase and the B2 phase is Ni-Al-rich phase. In general, the Ni-Al as well as Cr-Fe are the fundamental component phases of AlCrFe1.5Ni1.5 MEAs.

The chemical compositions of the constituent phases were summarized in Table 1. To ensure the accuracy of the measured results, each measurement was repeated 2 times and the average value was obtained. As Table 1 illustrated, the matrix phase was found to consist mainly of Ni (~24.8 at%) and Al

(~55.24 at%), but quite a few concentrations of Fe (~15.60 at%) are also dissolved in this phase. The large nanoparticle phase mostly contained Fe (~48.32 at%) and Cr (~37.99 at%), associated with the dissolution of Ni (~10.07 at%) and only small concentrations of Al dissolved in this phase. It can be deduced that the solution strengthening may play an important role in improving the strength of AlCrFe1.5Ni1.5 MEAs.

The high-resolution TEM (HRTEM) images of the AlCrFe1.5Ni1.5 MEAs were plotted in Fig. 4. From Fig. 4a, a coherent interface between the two phases, the AlNi-rich ordered B2 phase and FeCr-rich BCC phase were identified. The corresponding fast Fourier transform (FFT) patterns are shown in Fig. 4b and c. From the plot, the short range order in the B2 phase was identified. It was known that the B2 ordering tends to occupy the (000) and (1/2 1/2 1/2) atomic sites by specific atoms. Owing to the similar atomic radii and electronegativity, Fe and Ni tend to occupy one site of the B2 structure, while Al and Cr tend to occupy the other sites [38]. In this case, the lattice parameters of these two phases were determined, $a_{B2} = 0.2854$ nm and $a_{BCC} = 0.2869$ nm, respectively. As known, the lattice mismatch can be calculated by Eq.(1) [39]

$$\delta = 2(a_{B2} - a_{BCC}) / (a_{B2} + a_{BCC}) \quad (1)$$

Regarding the AlCrFe1.5Ni1.5 MEAs, the lattice mismatch was -0.52%, which suggests the coherent relationship between B2 and BCC phase. Overall, the coherent interface in the alloy can effectively hinder the dislocation motion and further enhance the mechanical properties.

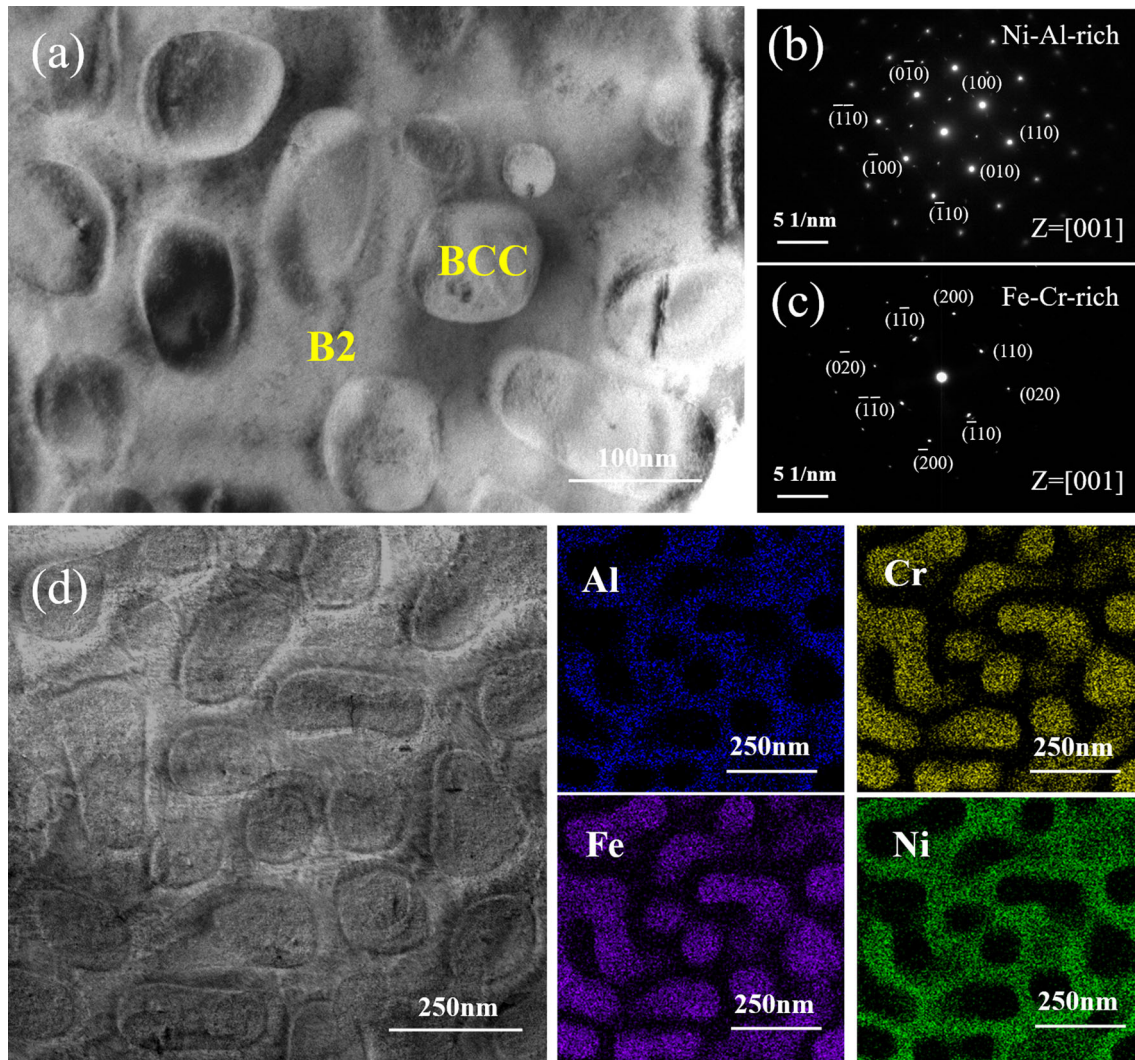


Figure 3 TEM analysis results of the AlCrFe1.5Ni1.5 MEAs. **a** Bright field image of the microstructure **b, c** SAED pattern of seed-like precipitates corresponding to BCC and B2 phase **d** Elemental distribution EDS maps.

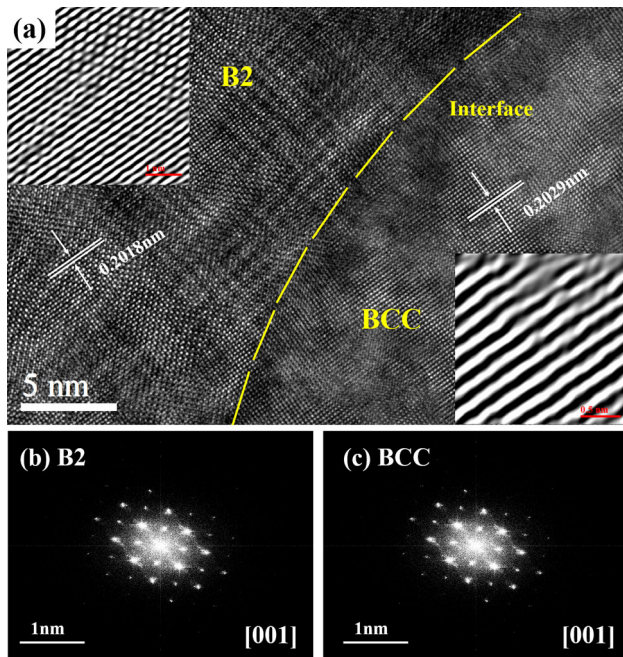
Mechanical property

The dependence of the mechanical properties on the test temperature is presented in Fig. 5. It can be deduced that the AlCrFe1.5Ni1.5 alloy displays the promising compressive strength and plasticity. Evidently at room temperature, the AlCrFe1.5Ni1.5 alloy exhibits exceptional plasticity (plastic strain > 40%), associated with the fairly high yield strength of 1231.64 MPa and fracture strength of 2172.79 MPa. As known, the typical AlCrFeCoNi HEAs [40] shows the yield stress, compressive strength and plastic strain of the alloy can reach 1250.96 MPa, 2004.23 MPa, and 32.7%, respectively. As such, the AlCrFe1.5Ni1.5 alloy exhibits fairly desirable combination of strength and plasticity compared with

AlCrFeCoNi alloy. When the temperature increases to 200 °C, the AlCrFe1.5Ni1.5 alloy also presents the reasonably high compressive strength as well as the unexpected plastic strain. The yield strength and fracture strength are 1201.09 MPa and 1987.96 MPa, respectively, accompanied with the plastic strain of 33.8%. Even at 400 °C, the AlCrFe1.5Ni1.5 alloy exhibits high fracture strength (>1500 MPa) and yield strength (>1000 MPa), as well as the fairly high plastic strain of 27.46%. It is rare for the HEAs/MEAs to produce such high strength at elevated temperature. As the temperature rises, the strength decreases significantly, but exhibits unexpected plastic strain. When the temperature was above 600 °C, the AlCrFe1.5Ni1.5 alloy prepared in this work exhibited

Table 1 Chemical compositions of each phase in AlCrFe1.5Ni1.5 MEAs

Phase	Chemical composition (at%)			
	Al	Cr	Fe	Ni
B2	24.8	4.38	15.60	55.24
BCC	7.26	37.99	48.32	10.07

**Figure 4** a HRTEM of the interface between B2 and BCC phases; The FFT patterns of b AlNi-rich ordered B2 phase and c FeCr-rich BCC phase.

great plasticity and was not broken with the strain above 70%.

In addition, a strong strain hardening ability was observed in AlCrFe1.5Ni1.5 alloy. The extremely pronounced work hardening stage can be observed overpass the yield stress, the work hardening behavior of AlCrFe1.5Ni1.5 alloy is expected to explore in depth. Herein, the experimental strain hardening behavior of AlCrFe1.5Ni1.5 alloy is analyzed using well-known empirical Hollomon equation, which can be used to critically fit the true stress-true strain data as follows [41].

$$\sigma = ke^n \quad (2)$$

where n presents the work hardening exponent. Taking the logarithm of the above equations and

differentiation of the logarithmic form of Eq. (3) with respect to ε provides:

$$\ln \sigma = \ln k + n \ln \varepsilon \quad (3)$$

Figure 5b plots the relationship of $\ln \varepsilon - \ln \sigma$ and the corresponding fitted curves at different temperatures. According, the fitting analysis show that the work hardening exponent n of AlCrFe1.5Ni1.5 alloy denotes 0.81 at room temperature. In terms of elevated temperature, there exists a slight decrease in the work hardening exponent. When the temperature increases to 200 °C, the n value decreases to 0.6. While, with the further increase of the temperature, the work hardening exponent of AlCrFe1.5Ni1.5 alloy fairly increases to 0.68, 0.76 and 1.63 at 400 °C, 600 °C and 800 °C, respectively. As the temperature increases to 1000 °C, the n value is determined as 0.38. As known, the higher n value usually indicates a exceptional formability. It is acceptable that the work hardening exponent of AlCrFe1.5Ni1.5 alloy is superior than the conventional metallic materials [42].

Besides this, as a crucial performance index, the work-hardening rate is also utilized to characterize the work hardening behavior in the homogeneous plastic deformation. The work-hardening rate θ can be expressed as

$$\theta = d\sigma/d\varepsilon \quad (4)$$

where σ represents the macroscopic true stress and ε corresponds to the strain. Figure 6 presents the true stress–strain curves of AlCrFe1.5Ni1.5 alloy at room and high temperature as well as the corresponding work hardening rate. Table 2 lists the true strength and the corresponding true strain of AlCrFe1.5Ni1.5 MEAs at both ambient and high temperatures. At ambient temperatures, the AlCrFe1.5Ni1.5 alloy presents the true strength of 1360.88 MPa as well as the high true strain of 35.44%. When the temperature increases to 200 °C, the true strength shows a slight decrease to the 1359.63 MPa, accompanied with true strain of 33.83%. Even the temperature increases to 400 °C, the true strength keeps above 1200 MPa. With a further increase of temperature to 1000 °C, the true strength decreases to 159.16 MPa, and no fracture can be observed. From Fig. 6, three typical stages can be observed in the process of deformation at room temperature. At first, it presents a rapid decrease of work-hardening rate at the initial stage which is

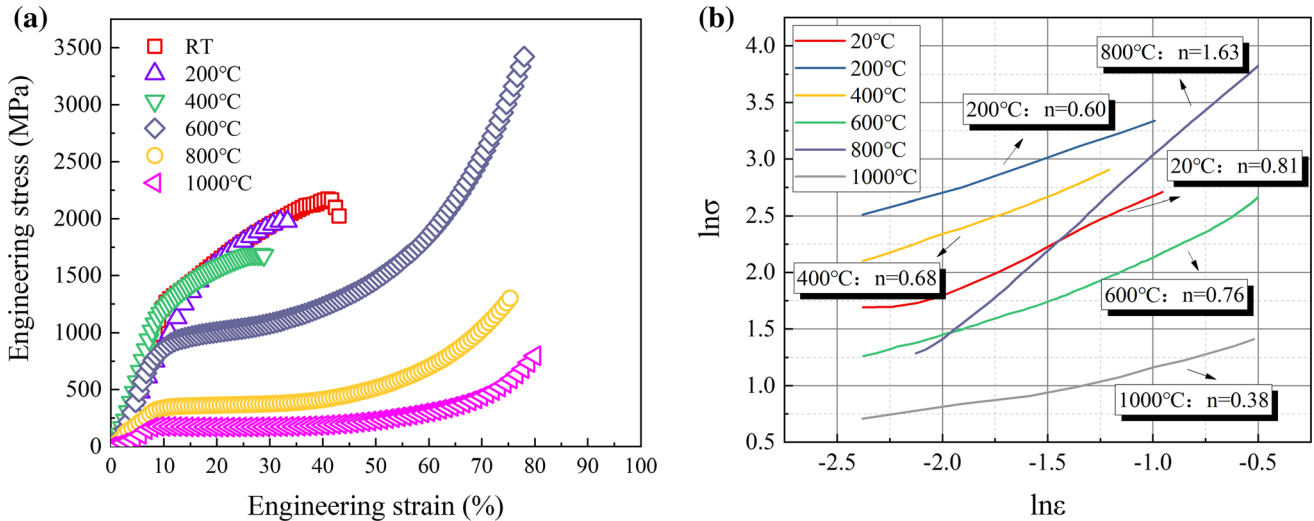


Figure 5 Engineering stress-strain curves by compressive tests **a** and the $\ln \varepsilon - \ln \sigma$ relationship **b** of the AlCrFe1.5Ni1.5 MEAs at room temperature and high temperature.

attributed to a short elastic-plastic transition. The annihilation and recombination of dislocations can be assumed in the deformation with the increasing strain [43]. Owing to the slip and climb motion of dislocations at grain boundaries, then it exhibits a slight increase in work-hardening rate. With the further increasing of true strain, it decreases gradually until finally the 0 value is reached. With high sensitivity to the temperature change, strain hardening in two stages is identified with respect to the elevated temperature. At 200 °C and 400 °C, it presents a rapid decrease of work-hardening rate at the initial stage and then shows a slight decrease. The great work hardening ability of AlCrFe1.5Ni1.5 alloy contributes to the flow stress as the strain increases. For 600 °C and 800 °C, it tends to be a stable value after an initial drop. Generally the work hardening behavior and dynamic softening mechanism are both involved in the deformation. When the hardening and softening mechanisms achieve dynamic equilibrium, it suggests a constant work-hardening rate. In particular, the high temperature always contributes to the dislocation slip and climb as well as the formation of dynamic recrystallization grains [44]. When the temperature increases to the 1000 °C, the work-hardening rate decreases rapidly to below 0 at the initial stage, indicating the predominance of softening mechanism. Then it increases slightly until an equilibrium is reached.

With respect to the strengthening mechanism of AlCrFe1.5Ni1.5 alloy under compression, it is

reasonable to suppose that this behavior is simply related to the formation of dual phases (disordered (BCC) and ordered (B2) bcc phases) in the multi-component alloy. As Fig. 4 plotted, there exists a high degree of coherence between the BCC and B2 phases, which contributes to the increasing strength at high temperature. The extra atoms of Ni can dissolve into the disordered [Fe, Cr] solid solutions except for combining with Al to form ordered B2 NiAl phases. Otherwise, the addition of Fe is assumed to dissolve into the B2 phase to produce a strong solid solution strengthening. Besides the lattice distortion caused by the Fe and Ni element, the amplitude-modulated decomposition structure of B2 phase can also improve its mechanical properties. Such that even at high temperature, the AlCrFe1.5Ni1.5 alloy exhibits desirable strength and superior plasticity. From the analysis above, the dual phase plays an important role in the enhancement of mechanical properties.

Toward the lightweight direction, the mechanical behavior can be assessed through the specific yield strength. Herein, the Archimedes drainage method was utilized to measure the density of the AlCrFe1.5Ni1.5 alloy. After repeated measurements, the average density denotes 6.75 g/cm^3 , which maintains the advantage of lightweight and can be comparable with nickel base superalloy with the density of about 8.0 g/cm^3 . The specific yield strength of AlCrFe1.5Ni1.5 alloy is $182.5 \text{ MPa}\cdot\text{cm}^3/\text{g}$ at room temperature. When the temperature increases to 200 °C, the specific yield strength shows a slight decrease

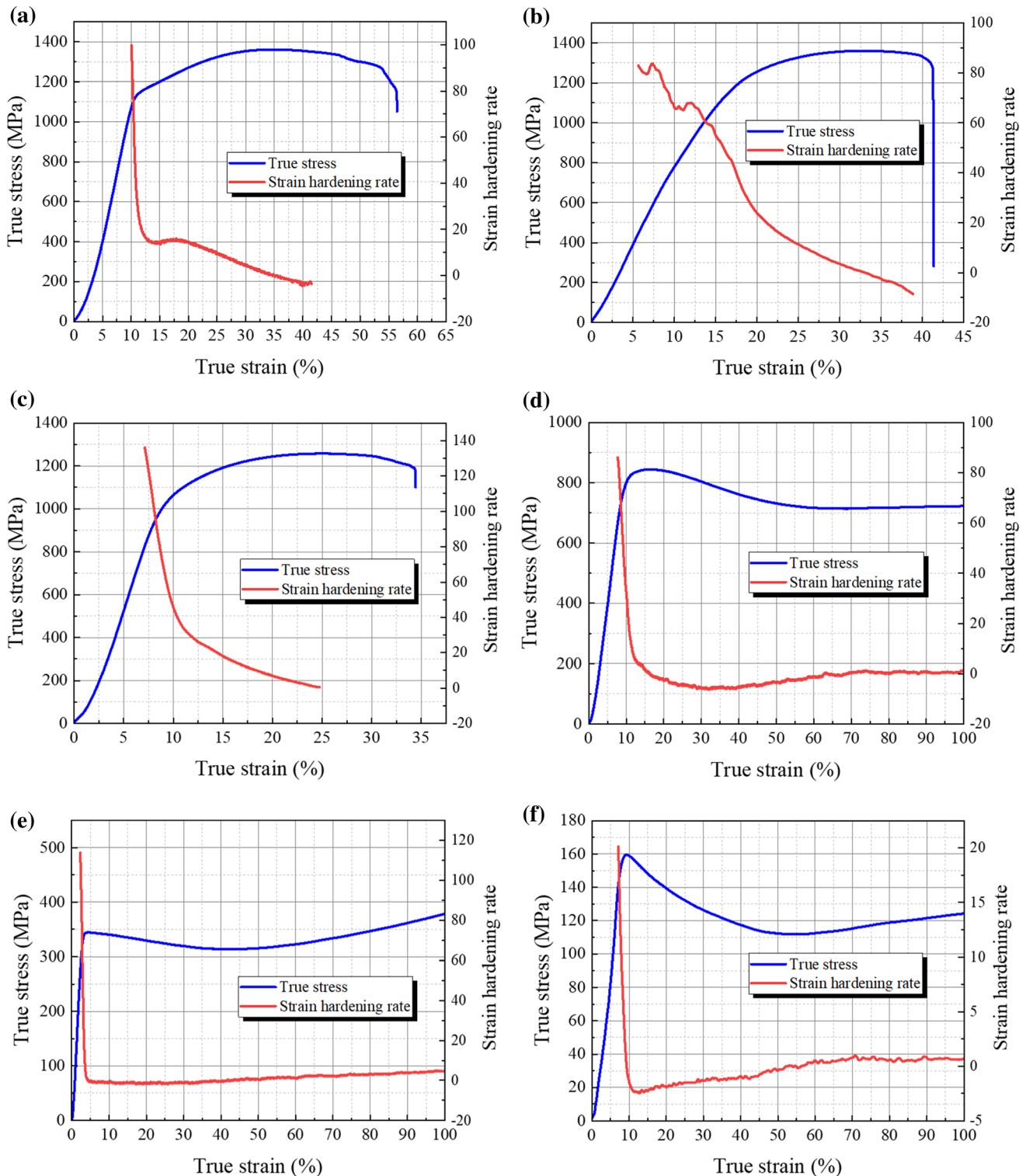


Figure 6 True stress–strain curves by compressive tests and strain hardening rate of AlCrFe1.5Ni1.5 alloy at **a** room temperature **b** 200 °C **c** 400 °C **d** 600 °C **e** 800 °C **f** 1000 °C.

and denotes $177.9 \text{ MPa}\cdot\text{cm}^3/\text{g}$. With the further increase of temperature, the yield strength of alloy decreases which results in the decreasing specific

yield strength. The specific yield strength of AlCrFe1.5Ni1.5 alloy is $157.4 \text{ MPa}\cdot\text{cm}^3/\text{g}$ and $122.3 \text{ MPa}\cdot\text{cm}^3/\text{g}$ at 400 °C and 600 °C, respectively.

Table 2 The true strength and corresponding true strain of AlCrFe1.5Ni1.5 MEAs

Temperature (°C)	True strength (MPa)	True strain (%)
20	1360.88	35.44
200	1359.63	33.83
400	1225.07	32.13
600	752.35	Not fracture
800	462.34	Not fracture
1000	159.16	Not fracture

When the temperature increases to 800 °C and 1000 °C, the specific yield strength decreases to 42.3 MPa·cm³/g and 25.9 MPa·cm³/g, respectively. Attribute to the high strength derived from dual-phase structure and the constituent of light element Al, the AlCrFe1.5Ni1.5 alloy exhibits extremely significant advantages in the specific yield strength compared with the conventional high-temperature structural alloys [45, 46] including titanium alloys and titanium aluminum alloys. Due to the excellent high temperature properties and low density, AlCrFe1.5Ni1.5 MEAs is attractive for use in aerospace field.

Friction and wear property

Friction coefficient and wear resistance

To evaluate the wear resistance, Fig. 7a demonstrates the COF curves of AlCrFe1.5Ni1.5 MEAs sliding against Al₂O₃ ball. With the sliding time, the curve rises sharply in the early stages and then reaches steady-state value, which assumes attributable to the change of contact state and wear mechanism during the process of wear test. Particularly some periodic waves with large fluctuation can be observed in the friction coefficient during steady-state stage, exhibiting close association with the periodic accumulation and elimination of the debris on the worn surface. The friction coefficient is expected to increase due to the accumulation of debris on the worn surface and then decrease when the debris is departed from worn surface and filled in the grinding cracks. The large

fluctuation can be observed for the AlCrFe1.5Ni1.5 alloy due to its high mechanical property and mild fracture on the worn surface.

Besides the friction measurements during dry sliding tests, the profilometry analysis and surface observation of wear tracks are used to quantitatively determine the wear behavior of AlCrFe1.5Ni1.5 MEAs. Figure 7b and c presents the 3D morphology of wear track and the schematic diagram of wear track profile. Based on the above information, the variation of the average friction coefficient, wear volume loss and wear width are summarized in Table 4. To estimate from values within steady range, the average friction coefficient is about 0.53. According to the macroscopic wear track morphology depicted in Fig. 8b, the wear width is quantitatively measured as 783.58 μm. During the wear process, the wear loss mainly derives from the plowing and micro-cutting by abrasive particles, e.g., which fallen from the sample surface and the tip of Al₂O₃ ball. Besides, the wear rate (K) is utilized to evaluate the wear resistance of AlCrFe1.5Ni1.5 alloy, which can be expressed as Eq. (4).

$$K = dV/F \times L \tag{5}$$

where V is the volume wear loss, F is the normal load, L is the sliding distance. As Table 3 illustrated, the measured wear volume is 0.89 × 10⁷ μm³ and the wear rate of the AlCrFe1.5Ni1.5 alloy denotes 0.71 × 10⁻⁵ mm³/(Nm). In general, the precipitation of a nano-sized BCC phase plays an important role in the hardness and wear resistance of the AlCrFe1.5Ni1.5 alloy. Besides, the solid solution strengthening resulted from the excess Fe and Ni atoms dissolved in the BCC/FCC phases can also contribute to the wear resistance of the AlCrFe1.5Ni1.5 alloy.

Worn surface and wear mechanism

For a further understanding, Fig. 8a displays the low magnification images of the wear scar for the as-cast AlCrFe1.5Ni1.5 MEAs. Subjected to the repetitive sliding, there is an obvious enhancement in the work-

Table 3 Average friction coefficient and wear rate of the AlCrFe1.5Ni1.5 MEAs

Sample	Wear rate (×10 ⁻⁵ mm ³ /(Nm))	Average friction coefficient	Wear width (μm)	Wear volume (×10 ⁷ μm ³)
AlCrFe1.5Ni1.5	1.97	0.53	783.58	0.89

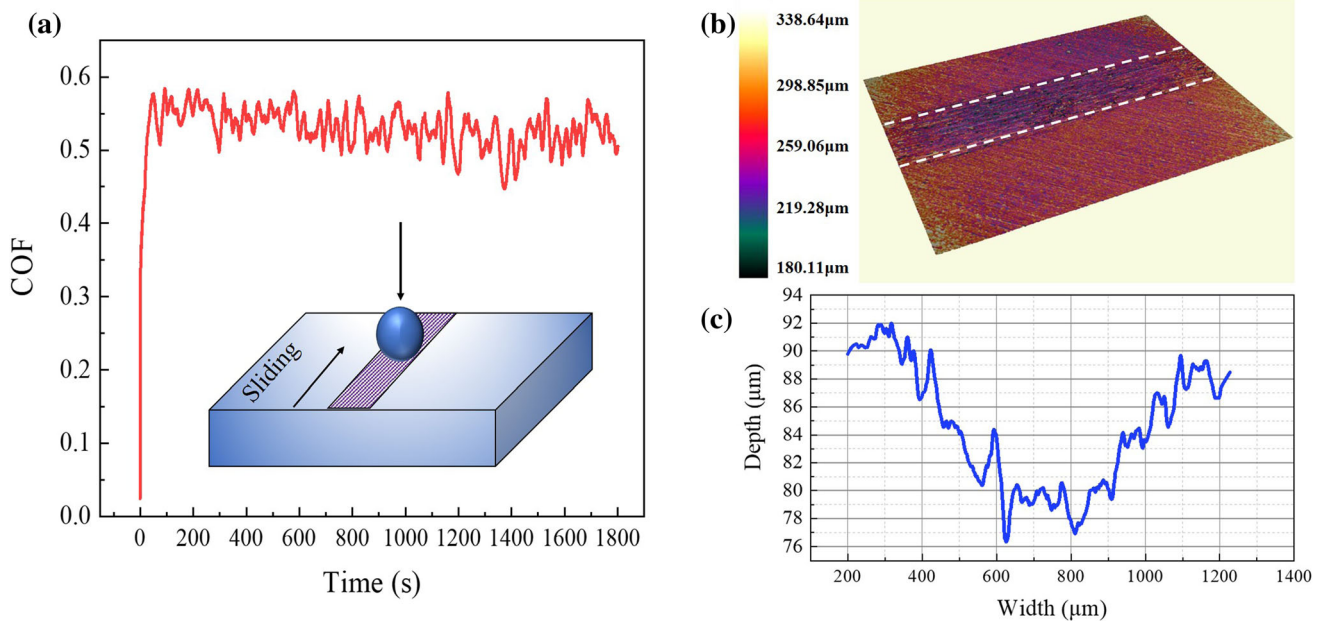


Figure 7 The wear track of AlCrFe1.5Ni1.5 MEAs **a** Friction coefficient **b** 3D morphology of wear track **c** The profile of the wear track.

Table 4 EDS analysis results for chemical composition (wt%) of wear debris

Sample	O	Al	Cr	Fe	Ni
AlCrFe1.5Ni1.5	7.67	8.79	19.22	31.60	32.72

hardening on the surface and then induces materials spalling on the surface. Evidently illustrated in Fig. 8b and d, some debris and wear particles can be observed on the worn surface of as-cast alloys. Owing to the micro-cutting, the hard wear particles tend to be embedded into the alloy surface and ploughed grooves during the sliding, as Fig. 8c illustrated. Thus, the worn surfaces of the samples display abrasive scratches and grooves parallel to the sliding direction, indicating the occurrence of abrasive wear. Besides, Fig. 8d and e presents the layered prows and delamination, indicating that the wear mechanism of AlCrFe1.5Ni1.5 MEAs involves adhesive wear. Fortunately, it can be observed that there is not visibly localized fracture on the worn surface.

In addition, Fig. 8f presents the micrographs of wear debris on the worn surface. The wear particles are all characterized by flakes with various shapes. It can be deduced that some oxidized particles are generated in the early stage of dry sliding. As the

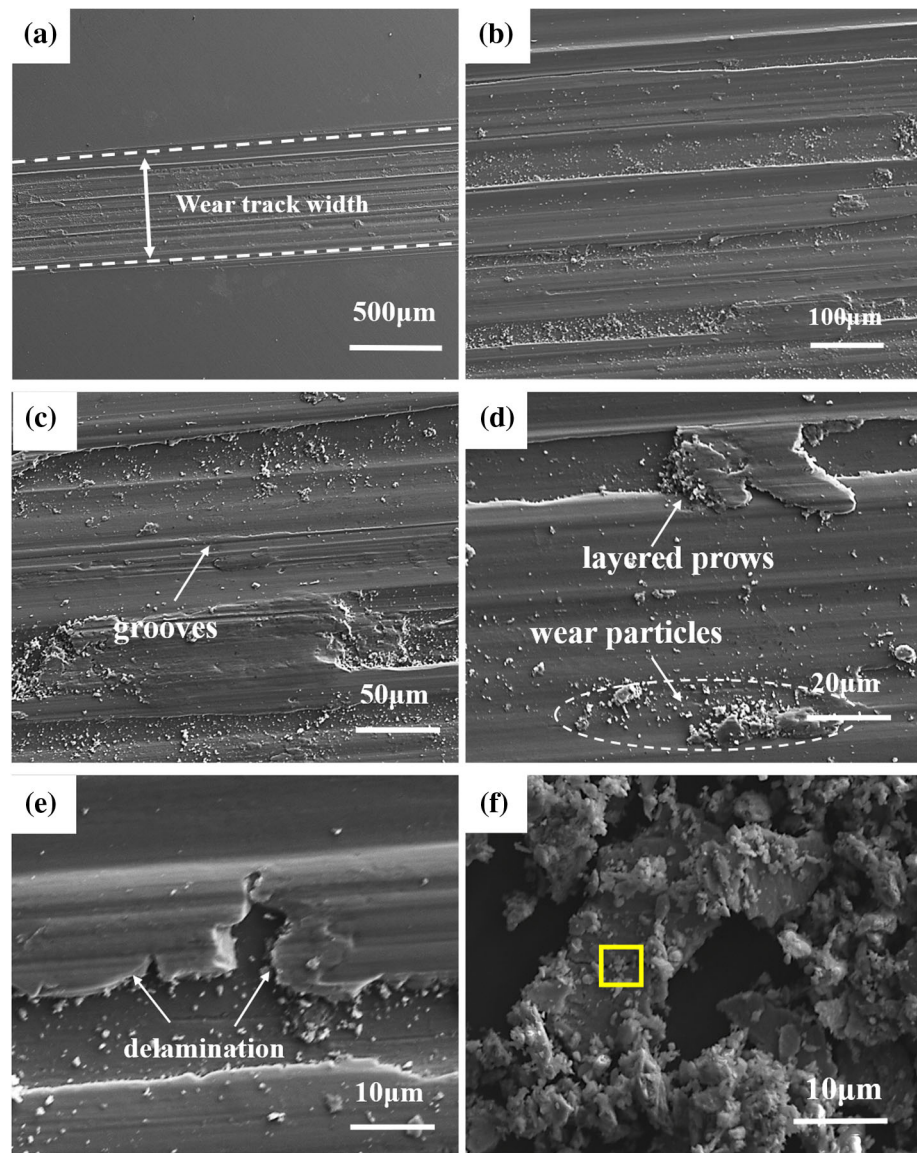
sliding continues, some oxidized particles are broken into smaller particles after undergoing further deformation and fragmentation. Eventually, a fraction of these oxidized particles can be removed from the wear track. The average chemical compositions of the debris are summarized in Table 4. It indicates the existence of oxides on the worn surface, which is attributed to the friction heat produced during the dry sliding. Owing to the formation of the smooth wear surface and the fine debris of high hardness, the addition of elements Fe and Ni can significantly improve the wear resistance of AlCrFe1.5Ni1.5 MEAs. Besides, the formation of the oxidative film can also limit the plastic deformation during the wear process. Thus, it can be deduced that the dominant wear mechanisms in the as-cast alloys involves the abrasive wear of oxide particles.

Conclusion

In this study, the AlCrFe1.5Ni1.5 MEAs were designed and prepared by vacuum arc melting techniques. The phase and microstructure, mechanical properties and wear resistance of the as-cast AlCrFe1.5Ni1.5 alloy have been discussed in detail. The conclusions can be drawn as follows:

- (1) The as-cast AlCrFe1.5Ni1.5 alloy consists of a disordered BCC-type [Fe, Cr] phase and an

Figure 8 EPMA micrographs of wear tracks of AlCrFe1.5Ni1.5 MEAs. **a**, **b** The micrographs of wear tracks at low magnification **c**, **d**, **e** The micrographs of wear tracks at low magnification **f** The micrograph of wear debris.



ordered B2 phase. The lamellar dendrite structure can be observed near the grain boundary and the spinodal decomposition of BCC phases can be identified in the grains. The dual phase of Al-Ni as well as Cr-Fe phases exhibit coherent relationship and play a major role in microstructures as well as properties.

- (2) The AlCrFe1.5Ni1.5 MEAs exhibit promising combinations of room temperature and elevated temperature mechanical properties. It shows a yield strength of 1231.64 MPa, an ultimate strength of 2172.79 MPa, and an exceptional plasticity (plastic strain > 40%) in the compressive condition. The true strength was 1360.88 MPa, accompanied with a high
- true strain of 35.44%. The Hollomon analysis indicates that it shows great work hardening ability and the work hardening behavior is systematically discussed from the plot of strain hardening rate. Attributed to the dual phase strengthening, the as cast AlCrFe1.5Ni1.5 alloy have such high strength and plasticity even at high temperatures. The low density of AlCrFe1.5Ni1.5 alloy arouses the high specific yield strength and promotes its application in aerospace field.
- (3) The AlCrFe1.5Ni1.5 MEAs exhibit superior wear resistance compared with conventional structural materials and some reported HEAs. The friction and wear tests indicate that the

average friction coefficient of the AlCrFe1.5Ni1.5 alloy is about 0.53 at dry sliding condition. The wear rate and wear loss volume can achieve only $1.97 \times 10^{-5} \text{mm}^3/(\text{Nm})$ and $0.89 \times 10^7 \mu\text{m}^3$. In particular, the wear mechanism of AlCrFe1.5Ni1.5 MEAs primarily involve abrasive wear and adhesive wear accompanied by oxidation wear.

Data availability

The data required to reproduce these findings cannot be shared at this time as the data also forms part of an ongoing study.

Declarations

Conflicts of interest The authors declare that they have no conflict of interest.

References

- [1] Yeh JW (2013) Alloy design strategies and future trends in high-entropy alloys. *JOM* 35(12):1759–1771
- [2] Yeh JW, Chen SK, Lin SJ, Gan JY, Chin TS, Shun TT, Tsau CH, Chang SY (2004) Nanostructured high-entropy alloys with multiprincipal elements—novel alloy design concepts and outcomes. *Adv Eng Mater* 6:299–303
- [3] George EP, Curtin WA, Tasan CC (2020) High entropy alloys: a focused review of mechanical properties and deformation mechanisms. *Acta Materialia* 188:435–474
- [4] Qiao L, Liu Y, Zhu J (2021) A focused review on machine learning aided high-throughput methods in high entropy alloy. *J Alloys Compd* 877:160295
- [5] Chen J, Zhou X, Wang W, Liu B, Lv Y, Yang Wei, Dapeng Xu, Liu Y (2018) A review on fundamental of high entropy alloys with promising high-temperature properties. *J Alloys Compd* 760:15–30
- [6] Zhang Y, Zuo TT, Tang Z, Gao MC, Dahmen KA, Liaw PK, Zhao Ping L (2014) Microstructures and properties of high-entropy alloys. *Prog Mater Sci* 61:1–93
- [7] Zhang W, Liaw PK, Zhang Y (2018) Science and technology in high-entropy alloys. *Sci China Mater* 61(1):2–22
- [8] Zhang L, Zhang Y (2020) Tensile properties and impact toughness of $\text{AlCo}_x\text{CrFeNi}_{3,1-x}$ ($x = 0.4, 1$) high-entropy alloys. *Front Mater* 7:92
- [9] Li R, Ren Z, Yuan W, He Z, Liaw PK, Ren J, Zhang Y (2021) Mechanical behaviors and precipitation transformation of the lightweight high-Zn-content Al-Zn-Li-Mg-Cu alloy. *Mater Sci Eng A* 802:140637
- [10] Ling Qiao RV, Ramanujan JZ (2022) Machine learning discovery of a new cobalt free multi-principal-element alloy with excellent mechanical properties. *Mater Sci Eng A* 845:143198
- [11] Qiao L, Bao A, Lai Z, Liu Y, Zhu J, Wang Y (2021) Alloy design and properties optimization of multi-component alloy based on solidification characteristics. *Mater Sci Eng A* 805:140576
- [12] Qiao L, Zhu J (2022) Constitutive modeling of hot deformation behavior of AlCrFeNi multi-component alloy. *Vacuum* 201:111059
- [13] Shi P, Zhong Y, Li Y, Ren W, Zheng T, Shen Z, Yang B, Peng J, Pengfei H, Zhang Y, Liaw PK, Zhu Y (2020) Multistage work hardening assisted by multi-type twinning in ultrafine-grained heterostructural eutectic high-entropy alloys. *Mater Today* 41:62–71
- [14] Yan X, Zhang Y (2020) Functional properties and promising applications of high entropy alloys. *Scr Mater* 187:188–193
- [15] Uporov SA, Ryltsev RE, Bykov VA, Kh Estemirova S, Zamyatin DA (2020) Microstructure, phase formation and physical properties of AlCoCrFeNiMn high-entropy alloy. *J Alloys Compd* 820:153228
- [16] Wang W, Wang J, Sun Z, Li J, Li L, Song X, Xiaodong Wen L, Xie XY (2020) Effect of Mo and aging temperature on corrosion behavior of $(\text{CoCrFeNi})_{100-x}\text{Mo}_x$ high-entropy alloys. *J Alloys Compd* 812:152139
- [17] Ye F, Jiao Z, Yan S, Guo L, Feng L, Jianxing Y (2020) Microbeam plasma arc remanufacturing: Effects of Al on microstructure, wear resistance, corrosion resistance and high temperature oxidation resistance of $\text{Al}_x\text{CoCrFeMnNi}$ high-entropy alloy cladding layer. *Vacuum* 174:109178
- [18] Qiao L, Ramanujan RV, Zhu J (2022) Effect of aluminum on the friction and wear behavior of Al_xCrFeNi medium-entropy alloys. *Adv Eng Mater* 2101475
- [19] Sünbül SE, İcin K, Şeren FZ, Şahin Ö, Çakıl DD, Sezer R, Öztürk S (2021) Determination of structural, tribological, isothermal oxidation and corrosion properties of Al-Co-Cr-Fe-Ni-Ti-Cu high-entropy alloy. *Vacuum* 187:110072
- [20] Yang T, Guo W, Poplawsky JD, Li D, Wang L, Li Y, Wangyu H, Crespillo ML, Yan Z, Zhang Y, Wang Y, Zinkle S (2020) Structural damage and phase stability of $\text{Al}_{0.3}\text{CoCrFeNi}$ high entropy alloy under high temperature ion irradiation. *Acta Mater* 188:1–15
- [21] Qiao L, Bao A, Wang Y, Liu Y, Lai Z, Zhu J (2020) Thermophysical properties and high temperature oxidation behavior of $\text{FeCrNiAl}_{0.5}$ multi-component alloys. *Intermetallics* 126:106899

- [22] Wang Y, Zhang M, Jin J, Gong P, Wang X (2020) Oxidation behavior of CoCrFeMnNi high entropy alloy after plastic deformation. *Corros Sci* 163:108285
- [23] Fang Y, Chen N, Du G, Zhang M, Zhao X, Cheng H, Wu J (2020) High-temperature oxidation resistance, mechanical and wear resistance properties of Ti(C, N)-based cermets with Al_{0.3}CoCrFeNi high-entropy alloy as a metal binder. *J Alloys Compd* 815:152486
- [24] Kim Y-K, Joo Y-A (2018) Hyoung Seop Kim, Kee-Ahn Lee, high temperature oxidation behavior of Cr-Mn-Fe-Co-Ni high entropy alloy. *Intermetallics* 98:45–53
- [25] Lu YP, Dong Y, Guo S, Jiang L, Kang HJ, Wang TM, Wen B, Wang ZJ, Jie JC, Cao ZQ, Ruan HH, Li TJ (2014) A promising new class of high-temperature alloys: eutectic high-entropy alloys. *Sci Rep* 4:6200
- [26] Dong Y, Gao X, Yiping L, Wang T, Li T (2016) A multi-component AlCrFe₂Ni₂ alloy with excellent mechanical properties. *Mater Lett* 169:62–64
- [27] Jumaev E (2021) Muhammad Aoun Abbas, Sang Chul Mun, Gian Song, Soon-Jik Hong, Ki Buem Kim, Nano-scale structural evolution of quaternary AlCrFeNi based high entropy alloys by the addition of specific minor elements and its effect on mechanical characteristics. *J Alloys Compd* 868:159217
- [28] Poulia A, Georgatis E, Lekatou A, Karantzalis AE (2016) Microstructure and wear behavior of a refractory high entropy alloy. *Int J Refract Metals Hard Mater* 57:50–63
- [29] Song H, Tian F, Hu Q-M, Vitos L, Wang Y, Shen J, Chen N (2017) Local lattice distortion in high-entropy alloys *Phys. Rev Mater* 1:023404
- [30] Archard JF (1953) Contact and rubbing of flat surfaces. *J Appl Phys* 24:981–988
- [31] Karakaş MS, Günen A, Çarboğa C, Karaca Y, Demir M, Altunay Y, Erdoğan A (2021) Microstructure, some mechanical properties and tribocorrosion wear behavior of boronized Al_{0.07}Co_{1.26}Cr_{1.80}Fe_{1.42}Mn_{1.35}Ni_{1.10} high entropy alloy. *J Alloys Compd* 886:161222
- [32] Gwalani B, Torgerson T, Dasari S, Jagetia A, Nartu MSKKY, Gangireddy S, Pole M, Wang T, Scharf TW, Banerjee R (2021) Influence of fine-scale B2 precipitation on dynamic compression and wear properties in hypo-eutectic Al_{0.5}CoCrFeNi high-entropy alloy. *J Alloys Compd* 853:157126
- [33] Du LM, Lan LW, Zhu S, Yang HJ, Shi XH, Liaw PK, Qiao JW (2019) Effects of temperature on the tribological behavior of Al_{0.25}CoCrFeNi high-entropy alloy. *J Mater Sci Technol* 35(5):917–925
- [34] Erdogan A (2021) Sefa Emre Sunbul, Kursat Icin, Kadir Mert Doleker, Microstructure, wear and oxidation behavior of AlCrFeNiX(X = Cu, Si, Co) high entropy alloys produced by powder metallurgy. *Vacuum* 187:110143
- [35] Qiao L (2020) Aorigele, Zhonghong Lai, Jingchuan Zhu, A promising new class of multi-component alloys with exceptional mechanical properties. *J Alloys Compd* 847:155929
- [36] Qiao L, Jingchuan Zhu Y, Teng AB, Lai Z, Wang Y (2021) Dynamic solidification model of low-density FeCrNiAl multi-component alloy. *Vacuum* 184:109873
- [37] Singh AK, Subramaniam A (2014) On the formation of disordered solid solutions in multi-component alloys. *J Alloy Compd* 587:113–119
- [38] Linden Y, Pinkas M, Munitz A, Meshi L (2017) Long-period antiphase domains and short-range order in a B2 matrix of the AlCoCrFeNi high-entropy alloy. *Scr Mater* 139:49–52
- [39] Lin L, Xian X, Zhong Z, Chen C, Zhu Z, Wu Y, Liaw PK (2020) *Intermetallics* 120:106744
- [40] Wang YP, Li BS, Ren MX, Yang C, Fu HZ (2008) Microstructure and compressive properties of AlCrFeCoNi high entropy alloy. *Mater Sci Eng A* 491(1–2):154–158
- [41] Zhao C, Chen X, Pan F, Gao S, Zhao D, Liu X (2018) Effect of Sn content on strain hardening behavior of as-extruded Mg-Sn alloys. *Mater Sci Eng A* 713:244–252
- [42] Shi Q, Wang C, Deng K, Nie K, Cao M, Gan W, Liang W (2020) Work hardening and softening behavior of pure Mg influenced by Zn addition investigated via in-situ neutron diffraction. *Mater Sci Eng A* 772:138827
- [43] Wen DX, Lin YC, Chen J, Chen XM, Zhang JL, Liang YJ, Li LT (2015) Workhardening behaviors of typical solution-treated and aged Ni-based superalloys during hot deformation. *J Alloy Compd* 618:372–379
- [44] Wang J, Liu Y, Liu B, Wang Y, Cao Y, Li T, Zhou R (2017) Flow behavior and microstructures of powder metallurgical CrFeCoNiMo_{0.2} high entropy alloy during high temperature deformation. *Mater Sci Eng A* 689:233–242
- [45] Lapin J (2009) TiAl-based alloys: present status and future perspectives. in: Proceedings of 18th international conference on metallurgy and materials metal-2009, Hradecnad Moravici, Czech Republic, pp 1-12
- [46] Senkov ON, Woodward C, Miracle DB (2014) Microstructure and properties of aluminum-containing refractory high-entropy alloys. *JOM* 66:2030–2042

Publisher's Note Springer Nature remains neutral with regard to jurisdictional claims in published maps and institutional affiliations.